

Supplementary Material

Hui-Ying Liu¹, Yue-Yi Wang¹, Ze-Yan Chen², Ting-Ping Hou^{1,2}, Kai-Ming Wu^{1,2}, and
Heng-Fu Lin^{1,2†}

¹Hubei Province Key Laboratory of Systems Science in Metallurgical Process, and
College of Science, Wuhan University of Science and Technology, Wuhan 430081,
China

²The State Key Laboratory for Refractory Material and Metallurgy, International
Research Institute for Steel Technology, and Collaborative Center on Advanced
Steels, Wuhan University of Science and Technology, Wuhan 430081, China

† Corresponding author. Email: hflin@wust.edu.cn (H. F. Lin).

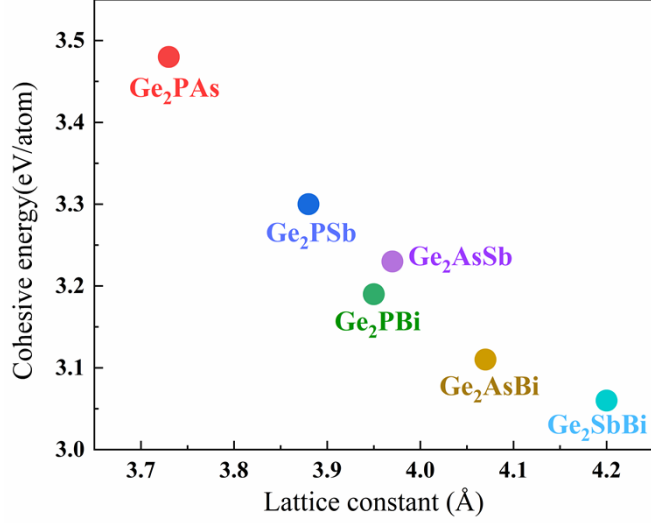


Figure S1. The variation of the cohesive energy with the lattice constant of the Janus α -Ge₂XY monolayers.

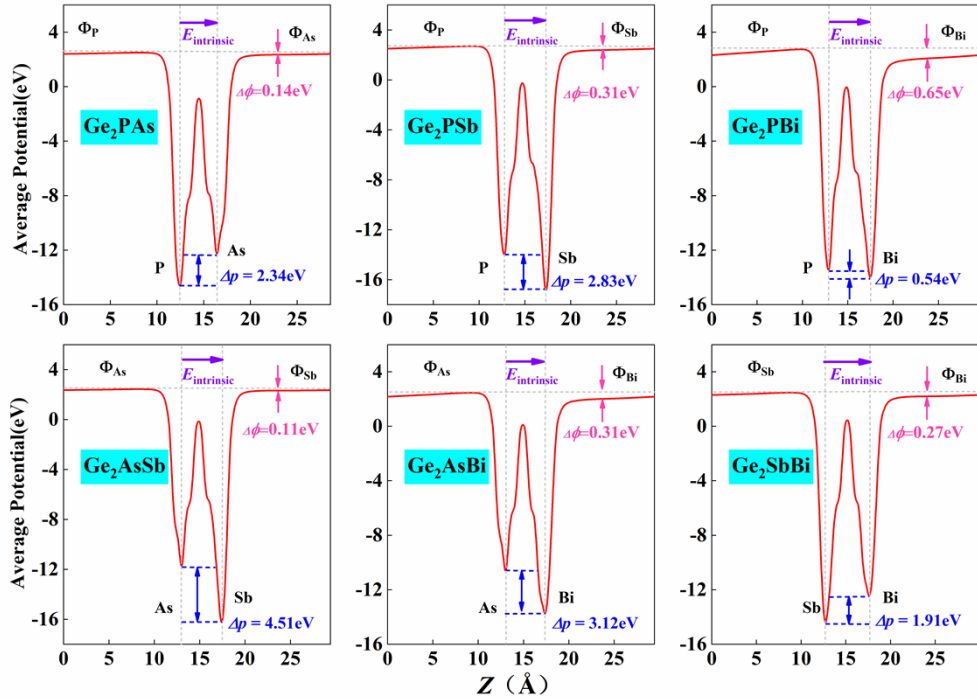


Figure S2. (a) Planar average of the electrostatic potential of Janus Ge₂XY monolayers along the z direction.

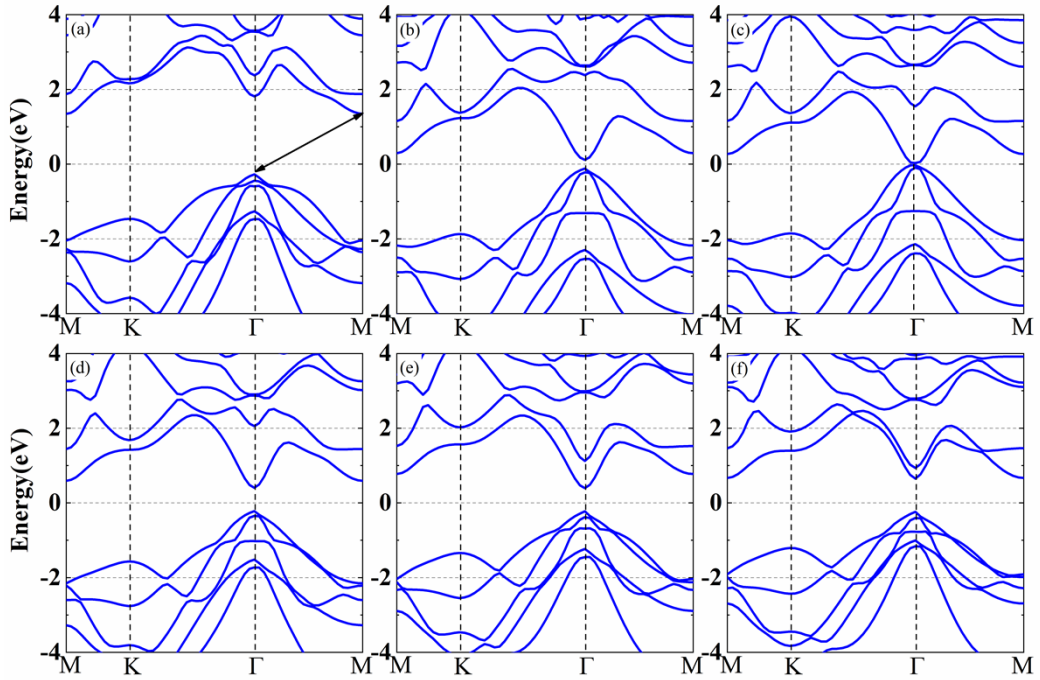


Figure S3. The HSE band structure of the Janus Ge_2XY monolayer, (a) Ge_2PAs , (b) Ge_2PSb , (c) Ge_2PBi , (d) Ge_2AsSb , (e) Ge_2AsBi , and (f) Ge_2SbBi . The Fermi level is set to zero energy.

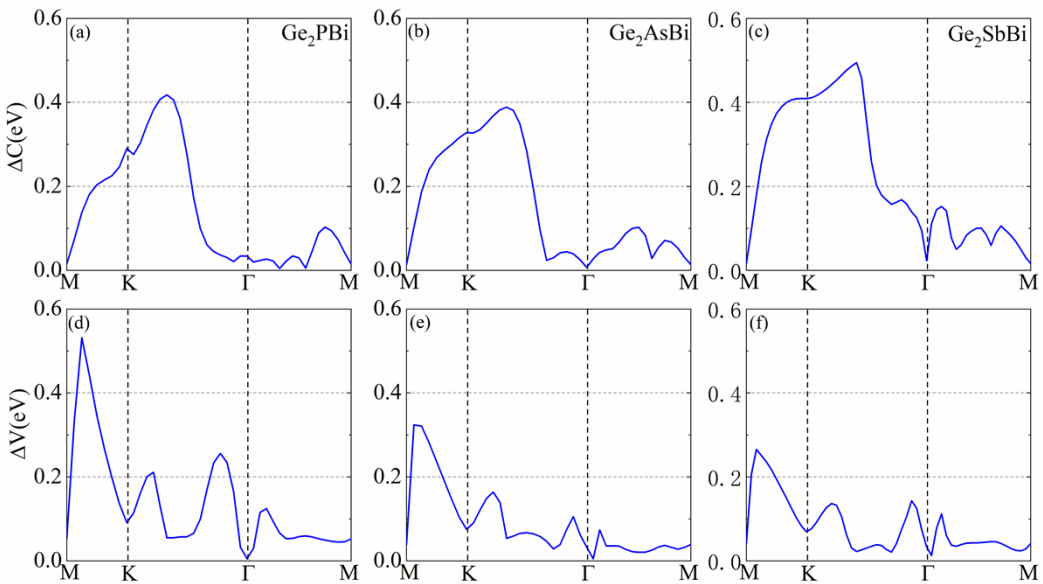


Figure S4. The magnitudes of the uppermost valence band spin splitting Δ_V and the lowermost conduction band spin splitting Δ_C along the $M\text{-}K\text{-}\Gamma\text{-}M$ line in the first Brillouin zone: (a) and (d) Ge_2PBi , (b) and (f) Ge_2AsBi , (c) and (e) Ge_2SbBi .

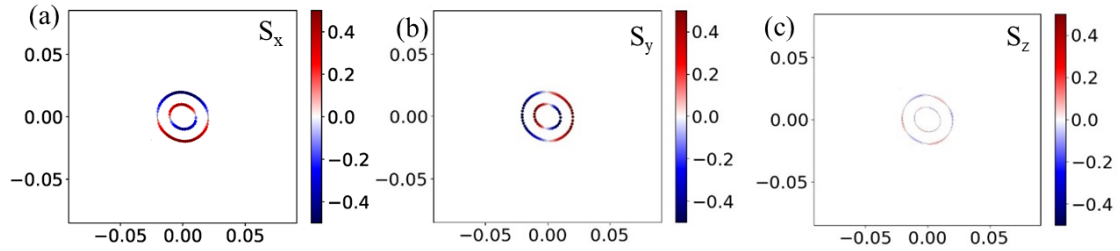


Figure S5. Spin textures of the upper and lower Rashba spin-orbit-splitting bands around Γ point of the Janus Ge_2AsBi . (a) S_x , (b) S_y , and (c) S_z components of the spin distribution at the constant energy contours above the Fermi level of 0.65 eV.

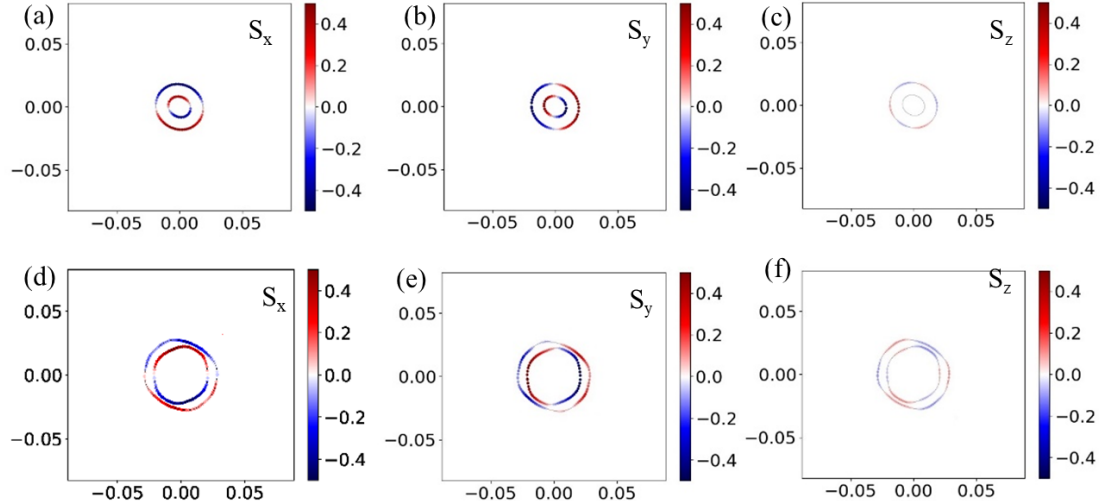


Figure S6. Spin textures of the upper and lower Rashba spin-orbit-splitting bands around Γ point of the Janus Ge_2SbBi . (a) S_x , (b) S_y , and (c) S_z components of the spin distribution at the constant energy contours above the Fermi level of 0.45 eV. (d) S_x , (e) S_y , and (f) S_z components of the spin distribution at the constant energy contours below the Fermi level of 1.00 eV.

Table S1. The calculated cohesive energy E_c and E_c^{vdw} of the Janus $\alpha\text{-Ge}_2XY$ and $\beta\text{-Ge}_2XY$ monolayers without and with considering the dispersive interaction (van der Waals interaction).

	$E_c(\text{eV/atom})$ (α)	$E_c(\text{eV/atom})$ (β)	$E_c^{\text{vdw}}(\text{eV/atom})$ (α)	$E_c^{\text{vdw}}(\text{eV/atom})$ (β)
Ge ₂ PAs	3.48	3.46	3.60	3.57
Ge ₂ PSb	3.30	3.27	3.41	3.37
Ge ₂ PBi	3.19	3.15	3.29	3.25
Ge ₂ AsSb	3.23	3.18	3.33	3.29
Ge ₂ AsBi	3.11	3.09	3.19	3.14
Ge ₂ SbBi	3.06	3.01	3.15	3.11

Table S2. The calculated formation energy E_{For} and $E_{\text{For}}^{\text{vdw}}$ of the Janus $\alpha\text{-Ge}_2XY$ and $\beta\text{-Ge}_2XY$ monolayers without and with considering the dispersive interaction (van der Waals interaction).

	$E_{\text{For}}(\text{eV/atom})$ (α)	$E_{\text{For}}(\text{eV/atom})$ (β)	$E_{\text{For}}^{\text{vdw}}(\text{eV/atom})$ (α)	$E_{\text{For}}^{\text{vdw}}(\text{eV/atom})$ (β)
Ge ₂ PAs	-3.95	-3.89	-4.07	-4.02
Ge ₂ PSb	-3.78	-3.70	-3.88	-3.81
Ge ₂ PBi	-3.66	-3.54	-3.78	-3.65
Ge ₂ AsSb	-3.71	-3.60	-3.82	-3.72
Ge ₂ AsBi	-3.58	-3.49	-3.67	-3.59
Ge ₂ SbBi	-3.51	-3.39	-3.60	-3.48

Table S3. The lattice constant (a and b), Ge-Ge bond length ($d_{\text{Ge-Ge}}$), and Ge- X bond length ($d_{\text{Ge-X}}$) of the non-Janus $\alpha\text{-Ge}_2X(Y)_2$ monolayers without considering the van der Waals interaction.

	$a(\text{\AA})$	$b(\text{\AA})$	$d_{\text{Ge-Ge}}(\text{\AA})$	$d_{\text{Ge-X}}(\text{\AA})$	$d_{\text{Ge-Y}}(\text{\AA})$
Ge ₂ P ₂	3.66	3.66	2.51	2.36	2.36
Ge ₂ As ₂	3.81	3.81	2.50	2.48	2.48
Ge ₂ Sb ₂	4.14	4.14	2.49	2.70	2.70
Ge ₂ Bi ₂	4.27	4.27	2.45	2.78	2.78

Table S4. The lattice constant (a and b), Ge-Ge bond length ($d_{\text{Ge-Ge}}$), Ge- X bond length ($d_{\text{Ge-X}}$), and Ge- Y bond length ($d_{\text{Ge-Y}}$) of the Janus monolayer $\beta\text{-Ge}_2XY$ without considering the van der Waals interaction.

	$a(\text{\AA})$	$b(\text{\AA})$	$d_{\text{Ge-Ge}}(\text{\AA})$	$d_{\text{Ge-X}}(\text{\AA})$	$d_{\text{Ge-Y}}(\text{\AA})$
Ge ₂ PAs	3.75	3.75	2.49	2.40	2.46
Ge ₂ PSb	3.89	3.89	2.48	2.46	2.62
Ge ₂ PBi	3.96	3.96	2.51	2.50	2.69
Ge ₂ AsSb	3.98	3.98	2.53	2.55	2.65
Ge ₂ AsBi	4.02	4.02	2.49	2.56	2.73
Ge ₂ SbBi	4.19	4.19	2.48	2.73	2.77

Table S5. The lattice constant (a and b), Ge-Ge bond length ($d_{\text{Ge-Ge}}$), and Ge- X bond length ($d_{\text{Ge-X}}$) of the non-Janus $\beta\text{-Ge}_2X_2$ monolayers without considering the van der Waals interaction.

	$a(\text{\AA})$	$b(\text{\AA})$	$d_{\text{Ge-Ge}}(\text{\AA})$	$d_{\text{Ge-X}}(\text{\AA})$
Ge ₂ P ₂	3.62	3.62	2.46	2.35
Ge ₂ As ₂	3.81	3.81	2.51	2.49
Ge ₂ Sb ₂	4.13	4.13	2.47	2.70
Ge ₂ Bi ₂	4.29	4.29	2.46	2.79

Table S6. The calculated Rashba energy(E_R), Rashba momentum offset (k_R), and Rashba coefficient (α_R) of the conduction and valence band near the fermi level of the Janus Ge₂XY monolayers.

	$E_R(\text{eV})$	$k_R(\text{\AA}^{-1})$	$\alpha_R (\text{eV}\cdot\text{\AA})$
Ge ₂ PBi (1)	0.0080	0.0125	1.28
Ge ₂ PBi (2)	0.0375	0.0400	1.87
Ge ₂ AsBi (1)	0.0120	0.0150	1.60
Ge ₂ SbBi (1)	0.0080	0.0100	1.60
Ge ₂ SbBi (2)	0.0250	0.0325	1.53

Table S7. The calculated elastic coefficients C_{ij} , in-plane Yong's modulus Y_{2D} , Poisson's ratio ν , piezoelectric stress coefficients e_{ij} , and the corresponding piezoelectric strain coefficients d_{ij} for the non-Janus Ge₂P₂, Ge₂As₂, Ge₂Sb₂, and Ge₂Bi₂ monolayers.

$C_{11}=C_{22}$ (N/m)	C_{12} (N/m)	Y (N/m)	ν	e_{11} ($10^{-10}\text{C}/\text{m}$)	e_{31} ($10^{-10}\text{C}/\text{m}$)	d_{11} (pm/V)	d_{31} (pm/V)
Ge ₂ P ₂	117	25	111.34	0.22	0.80	-	0.87
Ge ₂ As ₂	97	29	88.05	0.30	0.15	-	0.23
Ge ₂ Sb ₂	76	24	68.31	0.32	-1.14	-	-2.19
Ge ₂ Bi ₂	57	19	49.81	0.34	-1.62	-	-4.38